Technologies and Materials for Renewable Energy, Environment & Sustainability

# Study of the Alloy's Al-Cu-PbxZn10-x Performance in Attenuating Gamma Rays

AIPCP25-CF-TMREES2025-00002 | Article

# Study of the Alloy's Al-Cu-PbxZn$_{10-x}$ Performance in Attenuating Gamma Rays

Aya M. Ali Ismail [1,a)], Mahmood A. Hmood [1,b)] and Laith A. Najam [1,c)]

[1] *Department of Physics, Science College, University of Mosul, Mosul, Iraq*

[a)] *Corresponding author: ayamohammed19981995@gmail.com*
[b)] *dr.mahmood@uomosul.edu.iq*
[c)] *prof.lai2014@uomosul.edu.iq*

**Abstract.** The study focuses on studying the gamma-ray shielding performance of Al-Cu-Pb-Zn alloys, with an emphasis on their mass attenuation coefficients (MAC), half-value layer (HVL), and mean free path (MFP) in comparison to theoretical values. The study utilized three different alloy compositions: A1 ($Al_{67}Cu_{23}Pb_1Z_9$), A2 ($Al_{67}Cu_{23}Pb_2Z_8$), and A3 ($Al_{67}Cu_{23}Pb_3Z_7$), adjusting the proportions of aluminum (Al), copper (Cu), lead (Pb), and zinc (Zn) to assess their impact on gamma-ray attenuation. The findings indicated that the mass attenuation coefficient of the sample A3 was high (0.825 $cm^2/g$) at 60 keV due to its increased lead content that made it have dramatic radiation shielding efficacy. Conversely, sample, A1 recorded the lowest mass attenuation coefficient (0.072 $cm^2/g$) with a radiation of 662 keV. The mass attenuation coefficient was found to decrease gradually with increase of photon energy where Compton scattering becomes ineffective at higher energies. This pattern was not different to the theoretical prognoses attained utilizing the XCOM software to underscore the authenticity of the experimental setting. Besides, the HVL and MFP showed the negative correlation to the mass attenuation coefficient, and the greater concentrations of lead led to lower values found and indicated the increased shielding at decreased material thickness. The agreement between the experimental and theoretical calculations was quite high and particularly, in the immunological levels and mean free path, hence these alloys can effectively be used in gamma ray shielding applications. Also X-ray diffraction (XRD) and scanning electron microscopy (SEM) results showed the presence of different phases and elemental composition of alloys with the reason that they have radiation protective potential. On the whole, the results indicate that Al-Cu-Pb-Zn alloys, especially those with a larger amount of lead, have a viable possibility of use in radiation shielding.

**Keywords:** Alloys, Attenuation, Mass Attenuation Coefficient, XCOM, XRD Analysis, ESD Analysis and SEM Analysis.

## INTRODUCTION

Radiation refers to the energy emitted by different sources and travels through space as fast as light. It shapes various areas and offers different pros and cons [1]. On the positive note, radiation is often used for medical care, in factories, energy production and improving agriculture [2][3]. For instance, radiotherapy is very important in medicine, especially when treating cancer patients. If someone is exposed to radiation for long periods or in large amounts, it could increase their chance of developing cancers over the years [4]. To reduce the dangers caused by gamma rays, shielding materials have been developed for various types of ionizing radiation. There are many ways that these materials support the protection of humans and the environment from radiation. The denser a material is, the better its ability to shield [5]. Lead and concrete are commonly used to block radiation because they are highly effective at reducing it [6][7]. Because lead has a high atomic number, concrete can be obtained for low cost and all types of concrete are less harmful to the environment, they make excellent shields for gamma rays [8] Reducing radiation by using the correct kind of shields is extremely important [9]. Such materials act as stoppers that block most of the radiation and prevent workers from receiving too much radiation [10]. More technologies that produce ionizing radiation are being demanded, since medical fields and both industrial and commercial sectors are using them more often [11]. Frequently, doctors use X-rays and CT scanners for non-invasive tests, but ionizing radiation from them can be dangerous if they are not well-managed [12]. During the past few years, people have looked to alloys for radiation shielding because they have improved mechanical and chemical properties [13]. When different parts with unique shapes are joined in these materials, they become more resistant to rust, scratching and breaking [14]. Polymers can be used in many industries, including transportation, space, modern electronics and medicine [15]. Various analyses and experiments have been performed to measure the effectiveness of alloys in blocking gamma ray [16]. In radiation physics and dosimetry, a number of important parameters must be considered to understand how

radiation hits matter. These parameters consist of the mass attenuation coefficient, the effective atomic number, electron density, total cross section, half-value layer and mean free path. In particular, the mass attenuation coefficient explains the way matter responds to radiation [17][18]. In a study, Manjunatha et al. discovered that alloy (A160Y33N15C01Fe0.5Pd0.5) is suited for gamma shielding when compared to aluminum-based glassy alloys [19]. This work aims to build lightweight alloys and find the gamma photon attenuation coefficients of those alloys for use in radiation detection. They show suitable characteristics for shielding materials used in making ionizing radiation shields. A thallium-doped sodium iodide (TI) detector was used to measure the mass attenuation coefficients at photon energy levels from 60 keV to 662 keV. The experiments were checked against the XCOM program which calculated the mass attenuation coefficients of the tested alloys. The originality of this study lies in its investigation of the gamma-ray shielding properties of Al-Cu-Pb-Zn alloys, a material composition not frequently explored for this application. The research not only offers a comprehensive comparison of experimental results against the theoretical values predicted by XCOM software but also contributes to the growing body of work on advanced materials for radiation protection. The potential for these alloys in various industrial and medical applications is significant, considering their mechanical and chemical properties.

## EXPERIMENTAL PART

Three sets of Al-Cu-Pb-Zn alloys with unique compositions were formed in this study by melting the metals together in a gas furnace. The proportions of aluminum (Al), copper (Cu), lead (Pb), and zinc (Zn) in each sample were adjusted to investigate their effect on the alloy's gamma-ray shielding properties. The compositions of the alloys and their corresponding physical properties are presented in Table 1. This element was inserted first, in the crucible and then heated in the furnace because it has a high melting point of 1080 °C. The melting process of the copper took about 18 minutes. As a result, aluminum was inserted into the heated copper after reaching 660.3 °C. Lead and zinc were mixed in the last step and enclosed in a sheet of aluminum foil. After this was done, the mixture was placed inside a graphite vessel and put into the gas furnace. I kept the heating on for another 8 minutes to fully melt the example. The fully liquefied alloy was later cast into a wrought iron mold that was a cylinder with a diameter of 1 mm and a height of 3 cm. Gamma-ray absorption was measured using a narrow beam transmission set-up. The system uses a 2 x 2 inch NaI (Tl) scintillation crystal for detection. This crystal is energy-resolving to 6.3% at 173 Cs (662 KeV) and is attached to a multi-channel analyzer. The samples were placed 10 cm away from the radiation source, and the detector was always placed 20 cm from the source, as shown in Figure 1.

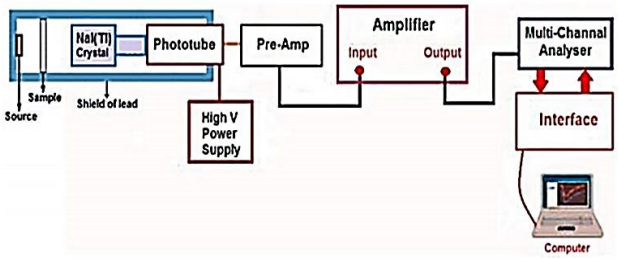


**FIGURE 1.** Illustrates the layout of the experimental work performed with the NaI (Tl) detector.

The Beer-Lambert law gives a way to work out the linear attenuation coefficient (LAC) which summarizes the chance of gamma ray interactions with a medium. Lambert-Beer talks about the linear attenuation coefficient ($\mu_L$) which refers to the decrease of photons in a beam passing through an absorber material [20] :

$$I = Io\ exp(-\mu Lx) \quad (1)$$

Io: stands for the initial unreduced intensity of photons, while I: is the attenuated level of photon intensity, X: refers to the thickness of the sample that was tested with μL: linear attention coefficient. Mass attenuation coefficient $\mu_m$ equals to linear attenuation coefficient divided by density of sample :

$$\mu m = \mu l/(\rho) \quad (2)$$

the density of the absorbent is labeled as $\rho$. It is in opposite proportion to the linear attenuation the Half-Value Layer (HVL) value is obtained by the relationship mentioned below[21] :

$$HVL = \frac{Ln_2}{\mu_L} \quad (3)$$

To calculate how fast rays enter a solid before energy transfer, the Mean Free Path (MFP) is needed and the formula used is :

$$MFP = \frac{1}{\mu_L} \quad (4)$$

**TABLE 1.** Display the chemical composition of alloys.

| Samples | Compounds | Mass(g) | Length (cm) | Diameter ($cm^2$) | Volume($cm^3$) | Thickness (cm) | Density (g $cm^{-3}$) |
|---|---|---|---|---|---|---|---|
| A1 | $Al_{67}Cu_{23}Pb_1Z_9$ | 17.36 | 6.46 | 1.2 | 7.30 | 0.3 | 4.62 |
| A2 | $Al_{67}Cu_{23}Pb_2Z_8$ | 18.74 | 6.71 | 1.2 | 7.60 | 0.3 | 4.66 |
| A3 | $Al_{67}Cu_{23}Pb_3Z_7$ | 19.14 | 6.45 | 1.2 | 8.46 | 0.3 | 4.70 |

## RESULTS AND DISCUSSION

A comparison was conducted between the experimentally obtained mass attenuation coefficients and the theoretical values calculated using the XCOM software, within a photon energy range of (1 keV - 100 Ge). The relationship between the experimental and theoretical data was illustrated graphically, as shown in Figure 2, highlighting the degree of consistency between the empirical measurements and the theoretical model. According to the data presented in Table 2, a gradual decrease in the mass attenuation coefficient (μ/ρ) is observed as the incident photon energy increases. This trend can be attributed to the dominance of the Compton scattering process. As photon energy rises, the cross-section of Compton scattering decreases, which in turn leads to a reduction in the mass attenuation coefficient due to the inverse relationship between the scattering cross-section and photon energy. A3 reached the highest mass attenuation coefficient, 0.825 $cm^2/g$ at 60 KeV, mostly because the alloy is made of elements with high atomic numbers. Sample A1 registered the smallest mass attenuation coefficient for 662 KeV radiation, coming out to 0.072 $cm^2/g$ .

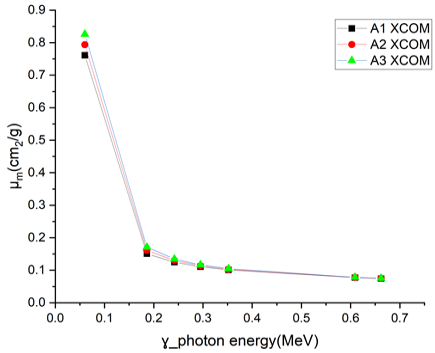


**FIGURE.2** Display both the experimental results and theoretical values from XCOM are shown for the mass attenuation coefficient (MAC) of alloy samples versus γ-photon energy.

**TABLE 2.** Details the mass attenuation coefficients $\mu_m$ ($cm^2$ /g) for all the alloys created by XCOM and those measured experimentally.

| Sample | Exp. Theor. | $\mu_m$ ($cm^2$ /g) | | | | | | |
|---|---|---|---|---|---|---|---|---|
| | | $Am^{241}$ | | | $Ra^{226}$ | | | $Cs^{137}$ |
| | | 60keV | 186kev | 242keV | 295keV | 352keV | 609keV | 662keV |
| **A1** | Exp. | 0.761 | 0.165 | 0.131 | 0.107 | 0.097 | 0.075 | 0.072 |

| | | | | | | | | |
|---|---|---|---|---|---|---|---|---|
| | XCOM | 0.761 | 0.150 | 0.124 | 0.110 | 0.101 | 0.077 | 0.074 |
| **A2** | Exp. | 0.794 | 0.172 | 0.137 | 0.112 | 0.101 | 0.078 | 0.075 |
| | XCOM | 0.793 | 0.160 | 0.129 | 0.113 | 0.102 | 0.077 | 0.074 |
| **A3** | Exp. | 0.825 | 0.179 | 0.143 | 0.117 | 0.105 | 0.082 | 0.081 |
| | XCOM | 0.826 | 0.171 | 0.134 | 0.116 | 0.104 | 0.078 | 0.075 |

**TABLE 3.** Shows the HVL from both XCOM and experiment methods.

| **Sample** | **Exp. Theor.** | **HVL (cm)** | | | | | | |
|---|---|---|---|---|---|---|---|---|
| | | **$Am^{241}$** | **$Ra^{226}$** | | | | | **$Cs^{137}$** |
| | | 60keV | 186keV | 242keV | 295keV | 352kev | 609keV | 662keV |
| A1 | Exp. | 0.197 | 0.907 | 1.136 | 1.389 | 1.540 | 1.986 | 2.081 |
| | XCOM | 0.197 | 0.994 | 1.202 | 1.351 | 1.484 | 1.935 | 2.014 |
| A2 | Exp. | 0.187 | 0.863 | 1.079 | 1.317 | 1.462 | 1.883 | 1.974 |
| | XCOM | 0.187 | 0.923 | 1.144 | 1.304 | 1.443 | 1.906 | 1.986 |
| A3 | Exp. | 0.178 | 0.822 | 1.028 | 1.255 | 1.394 | 1.791 | 1.883 |
| | XCOM | 0.178 | 0.860 | 1.092 | 1.259 | 1.404 | 1.878 | 1.958 |

Figures 3, experimental HVL is compared to the values predicted from theory by XCOM for alloys A1, A2 and A3 at energy Am241 at 60 keV, Ra226 at (242-295-352-699) keV and Cs137 at 662keV. Since there is an inverse connection between Mass attenuation coefficient and HVL, Figure. 3 reveals that the HVL increases with increasing γ-ray energy. Increasing γ-photon energy results in greater power to penetrate materials getting to that relation means I=50 Io%.

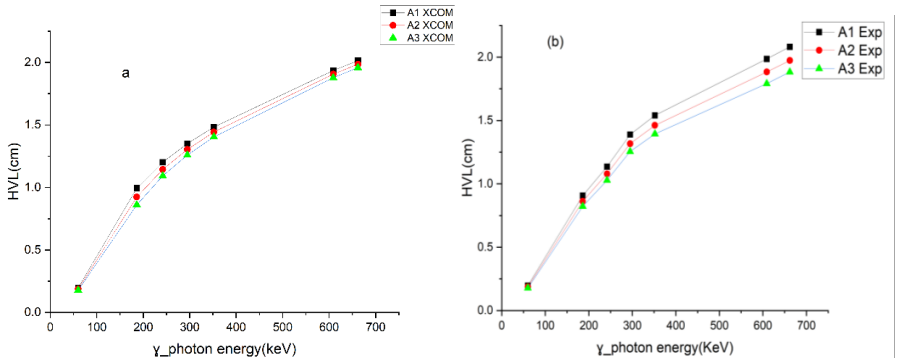


**FIGURE 3.** Shows how the Half-value layers (HVL) change (a) theoretical and (b) experiment for a set of alloy samples when the γ-ray energies vary.

**TABLE 4.** Illustrates the results of MFP from both XCOM and experiment methods.

| **Sample** | **Exp. Theor.** | **MFP (cm)** | | | | | | |
|---|---|---|---|---|---|---|---|---|
| | | **$Am^{241}$** | **$Ra^{226}$** | | | | | **$Cs^{137}$** |
| | | 60keV | 186keV | 242keV | 295keV | 352keV | 609keV | 662keV |
| A1 | Exp. | 0.284 | 1.309 | 1.639 | 2.004 | 2.222 | 2.865 | 3.003 |
| | XCOM | 0.284 | 1.434 | 1.734 | 1.950 | 2.141 | 2.792 | 2.906 |
| A2 | Exp. | 0.270 | 1.245 | 1.558 | 1.901 | 2.110 | 2.717 | 2.849 |

| | | | | | | | | |
|---|---|---|---|---|---|---|---|---|
| | XCOM | 0.270 | 1.332 | 1.651 | 1.881 | 2.082 | 2.751 | 2.865 |
| A3 | Exp. | 0.257 | 1.186 | 1.484 | 1.812 | 2.012 | 2.584 | 2.717 |
| | XCOM | 0.257 | 1.241 | 1.575 | 1.817 | 2.026 | 2.710 | 2.826 |

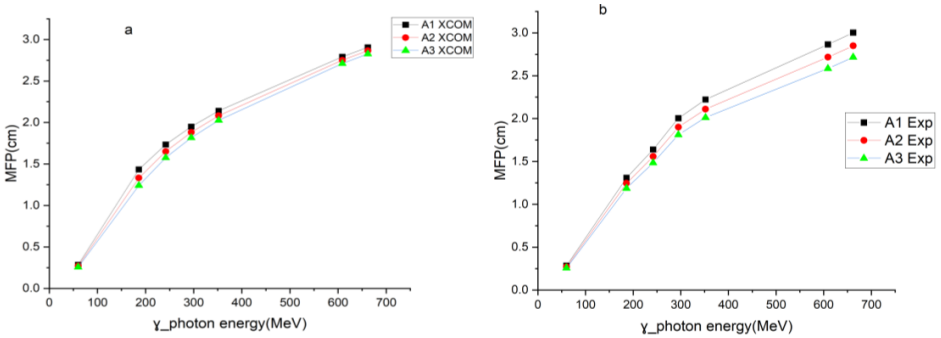


**FIGURE 4.** Illustrates the MFP of alloy samples together with changes in γ-ray energy (a)theoretical and (b) experimental.

Figure 4 illustrates the differences between the experimental data and the theoretical predictions of the mean free path (MFP) for all examined samples across the selected radiation source energies, as presented in Table 4. The findings reveal that MFP values are relatively low at lower energy levels and gradually increase as the energy rises. This behavior reflects the inverse relationship between the linear attenuation coefficient and the MFP. Overall, the comparison indicates a strong agreement between the experimentally measured and theoretically calculated values.

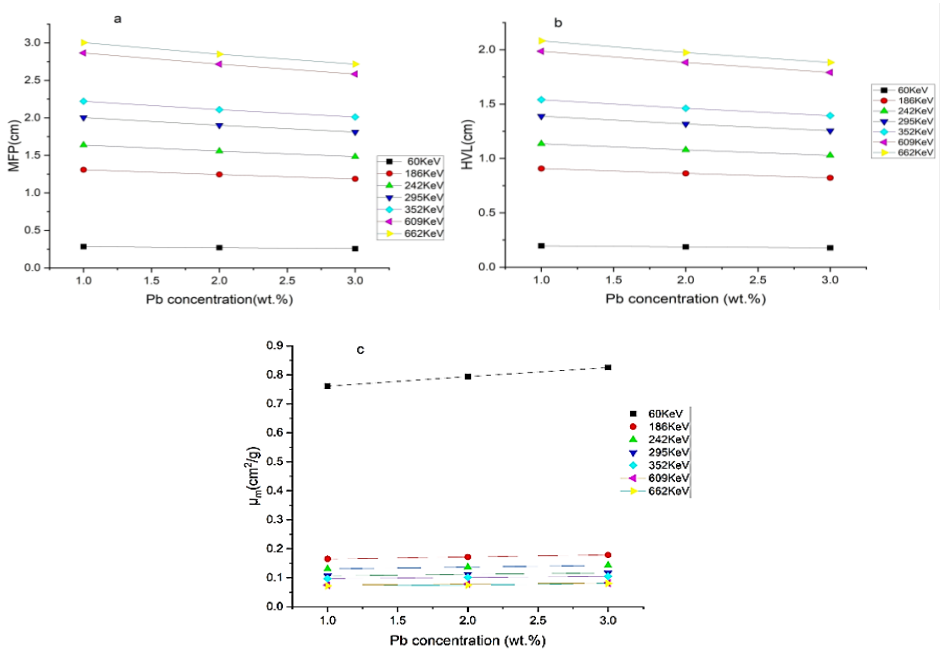


**FIGURE 5.** The influence of Pb concentration in (a) mass attenuation coefficient (MAC, $cm^2/g$, (b) Half value layer (HVL, cm), (c) MFP (cm).

The experimental results reveal that the mass attenuation coefficient (MAC) of alloy A3 at 60 keV is 0.825 $cm^2/g$, which is higher compared to the very low values of alloys A1 and A2. This higher

MAC can be attributed to the presence of lead in alloy A3. Lead is known for its ability to absorb gamma radiation due to its dense characteristics and large atomic number. These properties make lead particularly effective in gamma-ray attenuation, and the higher lead content in alloy A3 boosts its ability to shield radiation. This finding is consistent with previous studies, such as those by Sayyed et al. (2024) and Korkut et al. (2013), which confirm that elements with higher atomic numbers, like lead, are more efficient at attenuating gamma radiation. When compared to other materials used in radiation shielding, such as lead-based alloys or concrete, the performance of alloy A3 is competitive, especially at lower photon energies like 60 keV. The relationship between lead content and radiation shielding effectiveness is clear in the results. As seen in Figure 5(a), increasing the lead content in the samples leads to an increase in the mass attenuation coefficient, from 0.761 $cm^2/g$ to 0.825 $cm^2/g$, indicating better shielding. Figures 5(b) and (c) show that as the lead content rises, the half-value layer (HVL) and mean free path (MFP) decrease. Specifically, the HVL reduces from 2.081 cm to 1.883 cm, and the MFP decreases from 3.003 cm to 2.717 cm. These reductions suggest that alloy A3 provides better protection with a smaller thickness of lead.

Samples A1, A2 and A3 were examined by XRD device as shown in Figure 6. After analyzing the data, it was found that the samples contain major and minor phases according to the intensity of the peak and the angles at which the Braak condition is met. Figure 6 shows the presence of 3 major phases (Cu-Al), (Pb-Zn), (Al-Zn-Pb) at angles (38.8), (21), (42.7), (45) and (78.7) = 2θ, in addition to the presence of minor phases (Cu-Pd), (Cu-Zn) at angles (65.5), (48), (31.4), (29) = 2θ. SEM and EDS examinations were performed on the manufactured alloys A1, A2, and A3 to determine the surface structure and elemental composition of the sample. The EDS results in Figure 8 showed a range of elements including (Al) as the main element, in addition to (Cu), (Zn), and (Pb). This composition indicates that the sample belongs to multi-element aluminum alloys, which are known for their use in applications requiring improved mechanical properties and corrosion resistance. The EDS examination in Figure 9 revealed the appearance of light regions indicating the presence of lead and dark regions indicating the presence of aluminum, copper, and zinc. These results reflect a match between the microstructure and elemental composition of the sample, confirming the effectiveness of SEM and EDS techniques in characterizing metallic materials and studying the effect of mechanical and phase treatments on the surface structure.

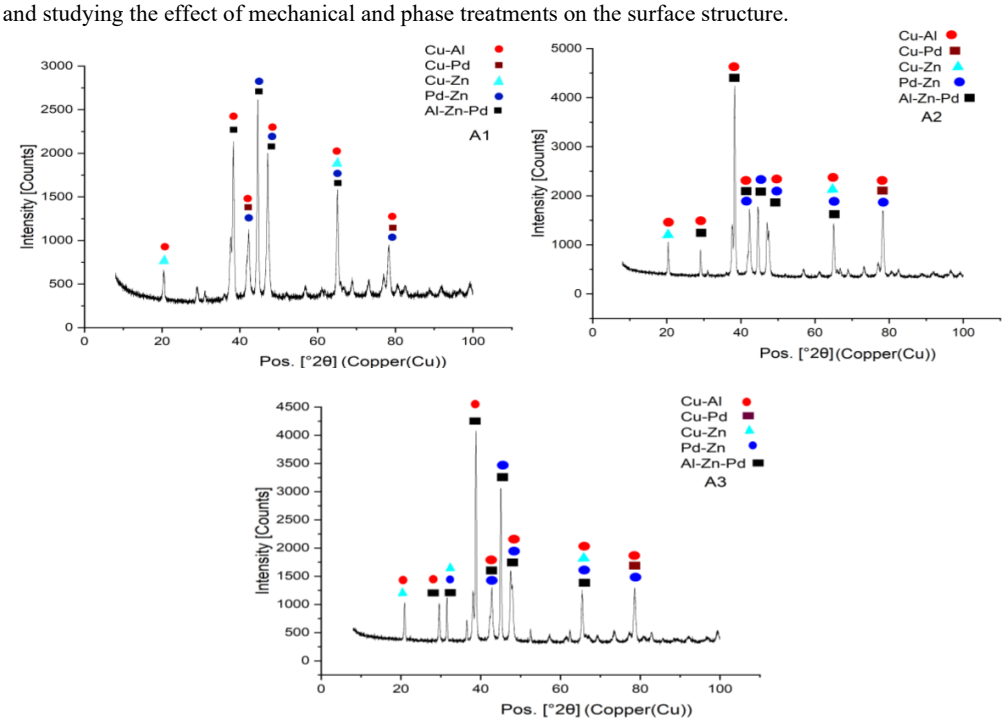


**FIGURE 6.** Illustrates the XRD analysis for alloy A1, A2 and A3.

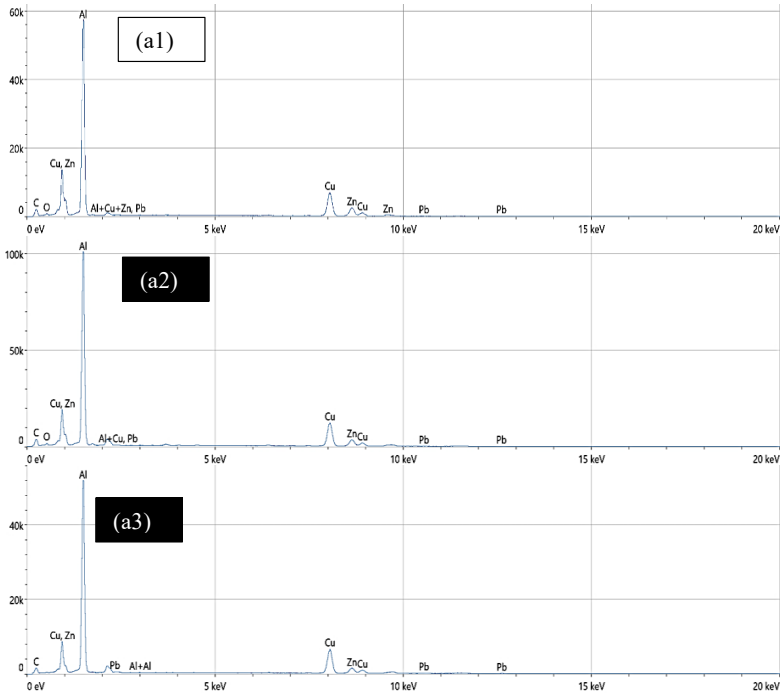


**FIGURE 7.** Display the ESD analysis for alloy a1, a2 and a3

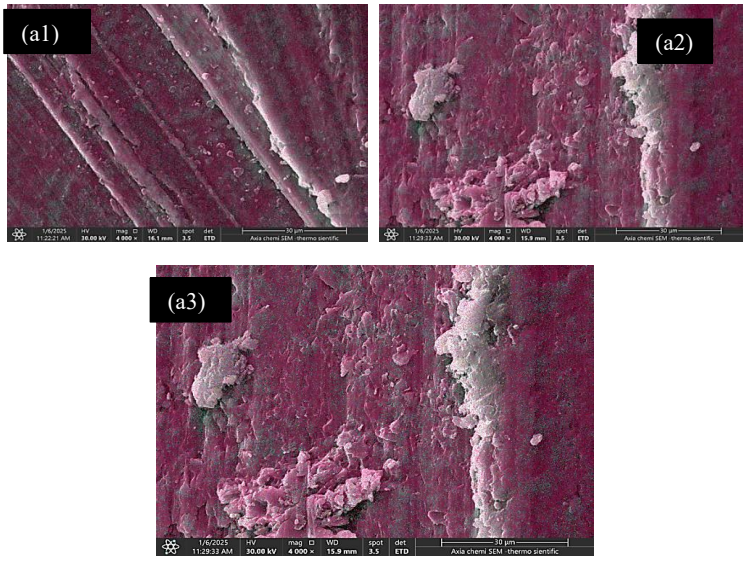


**FIGURE 8.** Show images of the surface of the a1, a2 and a3 alloy

## CONCLUSIONS

The results from this study highlight the effectiveness of Al-Cu-Pb-Zn alloys in shielding against gamma rays. Among the three alloys tested, alloy A3, which contained the highest amount of lead, showed the best performance in terms of gamma-ray attenuation. At 60 keV, its mass attenuation coefficient reached 0.825 cm²/g, which was significantly higher than that of alloys A1 and A2. In comparison, A1 had

a much lower value of 0.072 cm²/g at 662 keV, demonstrating a clear relationship between lead content and shielding effectiveness. The experimental measurements were compared with theoretical predictions from the XCOM software, and the results were in close agreement. This indicates that the experimental methods used were reliable, and the mass attenuation coefficients, half-value layers (HVL), and mean free paths (MFP) followed expected trends. As photon energy increased, the mass attenuation coefficients decreased, which is consistent with the nature of Compton scattering dominating at higher energies.

## REFERENCES


1. E. K. Ahmed, H. M. Mahran, M. F. Alrashdi, & M. Elsafi, "Studying the shielding ability of different cement mortars against gamma ray sources using waste iron and BaO microparticles," Nexus of Future Materials, vol. 1, pp. 1–5, 2024. [Online]. Available: https://nfmjournal.com/articles/3.
2. E. K. Ahmed and others, "Studying the shielding ability of different cement mortars against gamma ray sources using waste materials: Comparison study," Nexus of Future Materials, vol. 1, no. 1, pp. 1–5, 2024. [Online]. Available: https://nfmjournal.com/articles/3.
3. S. A. Abd El-Azeem and N. M. Harpy, "Radioactive attenuation using different types of natural rocks," Materials, vol. 17, no. 14, p. 3462, 2024. [Online]. Available: https://doi.org/10.3390/ma17143462.
4. T. Korkut, Z. I. Umaç, B. Aygün, A. Karabulut, S. Yapıcı, and R. Şahin, "Neutron equivalent dose rate measurements of gypsum-waste tire rubber layered structures," Int. J. Polym. Anal. Charact., vol. 18, no. 6, pp. 423–429, 2013.
5. R. Prasad, A. R. Pai, S. O. Oyadiji, S. Thomas, and S. K. S. Parashar, "Utilization of hazardous red mud in silicone rubber/mwcnt nanocomposites for high performance electromagnetic interference shielding," J. Clean. Prod., vol. 377, p. 134290, 2022.
6. M. I. Sayyed, "Radiation shielding properties of aluminosilicate glass systems using Phy-X software," J. Adv. Res. Appl. Sci. Eng. Technol., vol. 37, no. 2, pp. 156–164, 2024. [Online]. Available: https://doi.org/10.37934/araset.37.2.156164.
7. A. S. Altowyan, M. I. Sayyed, A. Kumar, and M. Rashad, "SrO–ZnO–PbO–$B_2O_3$ glassy insights: Unveiling the structural and optical features for gamma ray shielding efficacy," Opt. Mater., vol. 152, p. 115534, 2024. [Online]. Available: https://doi.org/10.1016/j.optmat.2024.115534.
8. K. Sarswat, S. K. Pal, Z. Y. Khattari, A. Dahshan, and N. Mehta, "A comprehensive study of radiation shielding parameters of chalcogens-rich quaternary alloys for nuclear waste management," Opt. Mater., vol. 157, no. 2, p. 116253, 2024. [Online]. Available: https://doi.org/10.1016/j.optmat.2024.116253.
9. H. Y. Zahran et al., "Radiation attenuation properties of the quaternary semiconducting compounds $Cu_2CoGe$ [S, Se, Te]$_4$," Results Phys., vol. 37, p. 105488, 2022. [Online]. Available: https://doi.org/10.1016/j.rinp.2022.105488.
10. K. A. Naseer, "Radiation shielding performance of bismuth–barium borate glasses: Structural and gamma-ray attenuation analysis," Nexus of Future Materials, vol. 2, pp. 177–181, 2025. [Online]. Available: https://doi.org/10.70128/593188.
11. A. Ajndal, "Mechanical and radiation shielding properties of $Bi_2O_3$–BaO–$V_2O_5$ glasses," J. Mater. Sci.: Mater. Electron., vol. 34, pp. 1746–.
12. K. M. Kaky, U. Altimari, and A. J. Kadhim, "Analytical and comparative study on the impact of CaO on the γ-ray shielding performance of borate-based glasses," Nexus of Future Materials, vol. 2, no. 2, pp. 172–176, 2025. [Online]. Available: https://doi.org/10.70128/S94252.
13. E. I. Majeed et al., "A comprehensive study on the γ-ray shielding performance of Al–Cu–PbO alloy: Experimental and simulation studies," Nucl. Eng. Technol., 2024. [Online]. Available: https://doi.org/10.1016/j.net.2024.07.055.
14. E. H. Abdel-Gawad, M. I. Sayyed, T. A. Hanafy, and M. Elsafi, "Experimental investigation of radiation shielding competence of $B_2O_3$ $Na_2O$ $Al_2O_3$ BaO CaO glass system," Sci. Rep., vol. 14, p. 14891, 2024. [Online]. Available: https://doi.org/10.1038/s41598-024-41569-1.
15. M. I. Sayyed, "Radiation shielding performance of amorphous silicates in the system $SiO_2$–$Na_2O$–RO (R = Cd, Pb or Zn)," Silicon, vol. 16, pp. 203–213, 2024. [Online]. Available: https://doi.org/10.1007/s12633-023-02607-x.
16. B. S. A. Bassam et al., "Physical, structural, elastic and optical investigations on $Dy^{3+}$ ions doped boro-tellurite glasses for radiation attenuation application," Radiation Phys. Chem., vol. 206, p. 110747, 2023. [Online]. Available: https://doi.org/10.1016/j.radphyschem.2023.110747.

17. M. I. Sayyed et al., "Uncovering the potential of ZnO and CaO in shielding and density enhancement for borate glass systems," Ann. Nucl. Energy, vol. 214, p. 111231, 2025. [Online]. Available: https://doi.org/10.1016/j.anucene.2025.111231.
18. H. J. Alasali et al., "Comparative analysis of $TiO_2$, $Fe_2O_3$, CaO and CuO in borate-based glasses for gamma ray shielding," Nucl. Eng. Technol., Advance online publication, 2024. [Online]. Available: https://doi.org/10.1016/j.net.2024.05.006.
19. C. Salame, F. Pelanchon, and P. Mialhe, “Degradation of VDMOSFETs by heavy ions irradiations,” Act. Passiv. Electron. Compon. 22, 265–282 (2000).
20. C. Salame and P. Mialhe, “N-channel power MOSFET for fast neutron detection,” Microelectron. Int. 19, 19–22 (2002).
21. M. I. Sayyed, K. A. Mahmoud, J. Arayro, Y. Maghrbi, M. H. A. Mhareb, "An extensive assessment of the impacts of BaO on the mechanical and gamma-ray attenuation properties of lead borosilicate glass," Sci. Rep., pp. 1–14, 2024. [Online]. Available: https://doi.org/10.1038/s41598-024-56040-2.